

# Metal-Doped Two-Dimensional Borophene Nanosheets for the Carbon Dioxide Electrochemical Reduction Reaction

Xuejian Xu, Xiuli Hou,\* Jiajie Lu, Peng Zhang, Beibei Xiao, and Jianli Mi



Cite This: <https://dx.doi.org/10.1021/acs.jpcc.0c05998>



Read Online

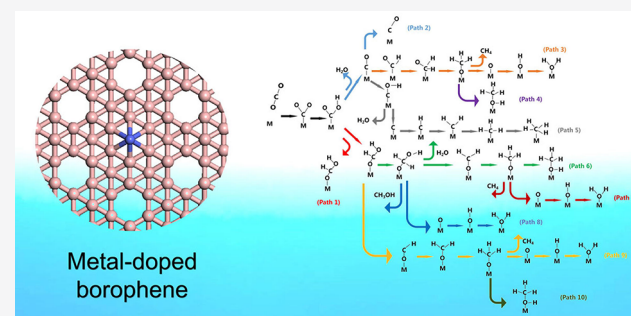
ACCESS |

Metrics & More

Article Recommendations

Supporting Information

**ABSTRACT:** Electrochemical reduction of carbon dioxide into hydrocarbons can promote the carbon dioxide utilization and decrease the greenhouse effect. In this work, the electrochemical reduction of carbon dioxide on metal-doped  $\alpha$ -borophene nanosheets was studied based on density functional theory. Our results show that the reduction of carbon dioxide on different metal-doped  $\alpha$ -borophene nanosheets proceeds through different preferred pathway. The free energies of the rate-determining step increase in the order of Co- = Fe- < Pd- < Pt- < Ni- < Rh- < Ru- < Ir- < Os-doped  $\alpha$ -borophene. A nearly linear relationship was observed between the reaction free energies of the rate-determining step and the adsorption energies of carbon dioxide on metal-doped  $\alpha$ -borophene nanosheets. Furthermore, the reduction of carbon dioxide was energetically more favorable than the hydrogen evolution reaction on Co- and Pd-doped  $\alpha$ -borophene nanosheets.



## 1. INTRODUCTION

Fossil fuels are continuously mined and burned, which emits large amounts of carbon dioxide ( $\text{CO}_2$ ) and accelerates global warming.<sup>1–3</sup> The catalytic conversion of  $\text{CO}_2$  to produce valuable chemicals has attracted immense attention.<sup>4</sup> This approach not only reduces atmospheric  $\text{CO}_2$  but also carries economic benefits. However,  $\text{CO}_2$  is one of the most stable carbon-based substances, and the electrochemical reduction of  $\text{CO}_2$  ( $\text{CO}_2\text{ERR}$ ) requires a large overpotential.<sup>5,6</sup> Therefore, many attempts have been made to develop electrocatalysts to speed  $\text{CO}_2\text{ERR}$ , including metals,<sup>7,8</sup> metal complexes,<sup>9</sup> metal-organic frameworks,<sup>10</sup> and metal-free catalysts.<sup>11</sup>

In recent years, many studies have found that single-metal atom catalysts (SACs) have outstanding catalytic performance. SACs consist of a support and isolated metal atoms/ions dispersed on the surface of the support, which makes the best use of the metal atoms and greatly improves the activity and selectivity of the catalysts.<sup>12–14</sup> Esrafil et al. found that Co could be stably doped in mono- or divalent defective nitrogen-doped graphene and then exhibited good performance for the conversion of  $\text{CO}_2$  to formic acid.<sup>15</sup> Zhao et al. found that single metal catalysts based on 2D InSe shows amazing  $\text{CO}_2\text{ERR}$  performance, among them,  $\text{CO}_2\text{ERR}$  on Cr@2DInSe prefers to form  $\text{CH}_4$  with a limiting potential of  $-0.36$  eV.<sup>16</sup> Jeong et al. used a simple method to synthesize single-atom nickel active sites on reduced graphene oxide (rGO) sheets as  $\text{CO}_2$  reduction reaction catalysts. Their results show that nitrogen-doped reduced graphene oxide sheets (Ni–N–rGO) exhibit a high  $\text{CO}_2$  reduction selectivity with a 97% Faradaic efficiency at  $-0.8$  V vs RHE.<sup>17</sup> Wang et al. studied TMN<sub>4</sub>/

graphene as a  $\text{CO}_2\text{ERR}$  catalyst using density functional theory (DFT) and found that CoN<sub>4</sub>/graphene, RhN<sub>4</sub>/graphene, and IrN<sub>4</sub>/graphene exhibited excellent catalytic activity.<sup>18</sup> Liu et al. investigated ten different transition metal-tetracyanoquinodimethane (TM-TCNQ) monolayers and found that Mn-TCNQs show the best performance with an overpotential of 0.12 V.<sup>19</sup>

Since the discovery of graphene,<sup>20,21</sup> many studies focused on two-dimensional materials.<sup>22</sup> Boron is near carbon in the periodic table and exhibits similar properties during the formation of planar clusters.<sup>23,24</sup> First-principles calculations first predicted the existence of two-dimensional boron materials.<sup>25</sup> Then a single boron monolayer (borophene) was synthesized on a silver substrate.<sup>26</sup> Borophene has many unique physical and chemical properties.<sup>27</sup> Its electronic band structure is highly anisotropic due to its highly anisotropic crystal structure. Moreover, borophene has also been reported to have superior catalytic properties.<sup>27</sup> Shen et al. reported that Cu atomic chains on  $\beta$ -borophene sheets show great catalytic activity for  $\text{CO}_2\text{ERR}$ , with overpotentials of 0.470 and 0.434 V for Cu<sub>4</sub>@B and Cu<sub>∞</sub>@B, respectively.<sup>28</sup> Liu et al. explored the catalytic performance of the nitrogen reduction reaction on 2D

Received: July 1, 2020

Revised: October 9, 2020

boron monolayers and found that the rate-determining step was the first reduction step with a  $\Delta G_{\max}$  of 0.77 eV.<sup>29</sup> Wang et al. studied the hydrogen storage performance of alkali-metal (Li, Na, and K)-doped borophene using first principle calculations and found that three types of Li-doped borophenes could be used for hydrogen storage.<sup>30</sup>

Now, a question arises: can transition metal-doped borophene catalyze CO<sub>2</sub> reduction? In this work, the possibility of  $\alpha$ -borophene nanosheets doped with nine different transition metal atoms (Fe, Co, Ni, Ru, Rh, Pd, Os, Ir, and Pt) for CO<sub>2</sub>ERR was studied based on DFT calculations.

## 2. COMPUTATIONAL METHODS

All spin-unrestricted calculations were performed within the DFT framework based on DMol<sup>3</sup> code.<sup>31</sup> The generalized

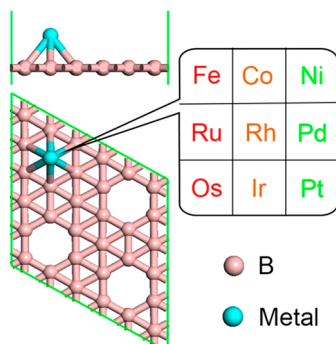


**Figure 1.** Atomic structure of metal-doped borophene nanosheets.

gradient approximation (GGA) with PW91 was employed to characterize the exchange and correlation functionals.<sup>32</sup> All-electron relativistic core treatment was used for relativistic effects.<sup>33</sup> The double numerical plus polarization (DNP) basis set was implemented for atomic orbitals.<sup>31</sup> A smearing value of 0.005 Ha was used to accelerate the electronic convergence. The real space global orbital cutoff radius was set to 5.2 Å to ensure high-quality results. van der Waals interactions were described by DFT + D2 method throughout all calculations.<sup>34</sup> The convergence tolerances of energy, maximum displacement, and maximum displacement were  $1.0 \times 10^{-5}$  Ha, 0.005 Å, 0.002 Ha/Å, respectively.

In this work, the CO<sub>2</sub>ERR catalytic activities of borophene doped with nine different transition metals (Fe, Co, Ni, Rh,

Ru, Ir, Ni, Pd, and Pt) were examined systematically (Figure 1). In this work, several different adsorption sites of transition metals on borophene nanosheets have been examined and only the most stable site is shown in this manuscript. Figure S1 shows the most stable adsorption site of Co on borophene. To prevent the interaction between metal-doped borophene, the distance between metal-doped borophene nanosheets and their mirror images was set to 20 Å. The optimized lattice constants for Fe-, Co-, Ni-, Ru-, Rh-, Pd-, Os-, Ir-, and Pt-doped borophene were  $10.1 \times 10.1 \times 20$ ,  $10.2 \times 10.2 \times 20$ ,  $10.2 \times 10.2 \times 20$ ,  $10.2 \times 10.2 \times 20$ ,  $10.1 \times 10.1 \times 20$ ,  $10.2 \times 10.2 \times 20$ ,  $10 \times 10 \times 20$ ,  $10.1 \times 10.1 \times 20$  and  $10.3 \times 10.3 \times 20$  Å<sup>3</sup>, respectively. The adsorption energy ( $E_{ad}$ ) of reaction intermediates was calculated as  $E_{ad} = E_{mol} + E_{metal-doped-borophene} - E_{mol-metal-doped-borophene}$ <sup>35</sup> where  $E_{mol}$ ,  $E_{metal-doped-borophene}$ , and  $E_{mol-metal-doped-borophene}$  represent the electronic energies of the isolated CO<sub>2</sub>ERR intermediate molecule, the metal-doped borophene nanosheet, and the adsorption system, respectively.<sup>36</sup> A positive  $E_{ad}$  value represents an exothermic adsorption process. The reaction free energy ( $\Delta G$ ) of every elementary step during CO<sub>2</sub>ERR was calculated based on the computational hydrogen electrode (CHE) model.<sup>37</sup> The  $\Delta G$  value was calculated as  $\Delta G = \Delta E + \Delta ZPE - T\Delta S$ ,<sup>38,39</sup> where  $\Delta E$  was the change of total energy,  $\Delta ZPE$  was the change of the zero-point energy,  $\Delta S$  was the change of entropy, and  $T$  was the temperature and was set as 298.15 K.<sup>40</sup> The conductor-like screening model (COSMO) was used to simulate the aqueous environment, and the dielectric constant was set to 78.54.<sup>41</sup>

## 3. RESULTS AND DISCUSSION

The favorable adsorption property of CO<sub>2</sub> is a prerequisite for CO<sub>2</sub>ERR on metal-doped borophene nanosheets. As CO<sub>2</sub> cannot adsorb on pristine borophene stably (Figure S2 in Supporting Information), it is necessary to enhance the adsorption of CO<sub>2</sub> on borophene through doping by transition metals. Figure 2(a) shows the classical adsorption structure of the CO<sub>2</sub> molecule on Co-doped borophene. It was found that CO<sub>2</sub> adsorbed on a Co atom with a curved configuration with an adsorption energy of 0.36 eV, indicating that CO<sub>2</sub> can adsorb on the surface of Co-doped borophene stably. The hybridization between Co-3d and the electronic states of CO<sub>2</sub> contributed to the stable adsorption of CO<sub>2</sub> on Co-doped borophene (Figure 2(b)). According to the Sabatier principle,<sup>42</sup> too strong or too weak adsorption energy is negative for the catalytic performance. Li and Yang's group

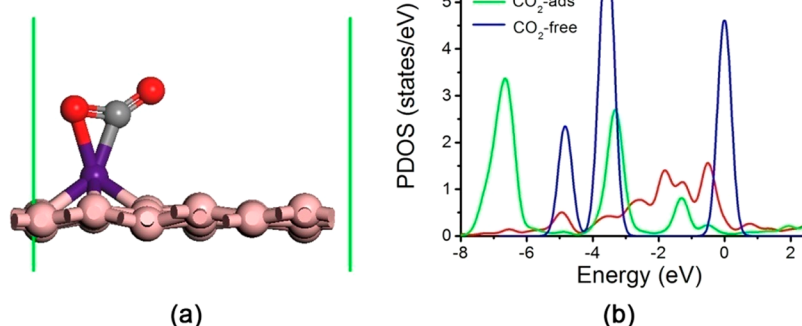


**Figure 2.** Adsorption structure (a) and PDOS (b) of CO<sub>2</sub> on Co-doped borophene.

**Table 1.** Adsorption Energies ( $E_{ad}$ ) of the CO<sub>2</sub>ERR Intermediates (CO<sub>2</sub>, COOH, CO, CHO, CH<sub>2</sub>O, CH<sub>3</sub>O, O, OH, COH, C, CH, CH<sub>2</sub>, CH<sub>3</sub>, HCOOH, OCH<sub>2</sub>OH, and OCH) on Metal-Doped Borophene Nanosheets (all results are in units of eV)

	CO <sub>2</sub>	COOH	CO	CHO	CH <sub>2</sub> O	CH <sub>3</sub> O	O	OH
Fe/B	0.51	2.71	2.39	3.31	1.33	2.85	5.60	3.33
Co/B	0.36	2.44	2.04	3.11	1.16	2.73	4.39	3.06
Ni/B	0.46	2.45	1.92	2.33	1.30	2.71	3.93	3.07
Ru/B	0.79	2.97	2.24	2.81	1.33	3.57	5.77	3.91
Rh/B	0.59	2.8	1.82	2.78	1.32	2.97	4.38	3.32
Pd/B	0.2	2.17	1.55	2.01	1	2.39	3.26	2.77
Os/B	1.53	3.54	3.34	3.38	2.57	4.19	7.37	4.58
Ir/B	1.13	3.42	2.88	3.34	1.97	3.57	5.72	3.91
Pt/B	0.68	3.05	2.61	2.96	1.47	2.96	4.52	3.35
	COH	C	CH	CH <sub>2</sub>	CH <sub>3</sub>	HCOOH	OCH <sub>2</sub> OH	OCH
Fe/B	3.75	5.84	5.45	3.69	2.31	0.89	2.73	0.77
Co/B	3.38	4.93	4.53	3.1	2.15	0.56	3.09	0.25
Ni/B	2.83	3.65	3.80	3.00	2.11	0.78	3.03	2.73
Ru/B	4.52	6.43	5.77	4.21	2.67	1.01	3.85	0.82
Rh/B	3.4	5.23	4.58	3.52	2.43	0.81	2.75	2.91
Pd/B	1.67	3.13	3.22	2.57	1.52	0.67	2.08	1.67
Os/B	5.33	7.38	7.33	5.16	3.12	1.27	4.61	1.32
Ir/B	4.74	6.72	6.34	4.67	3.05	1.04	3.39	3.28
Pt/B	3.84	5.27	5.16	4.03	2.71	0.72	2.45	1.45

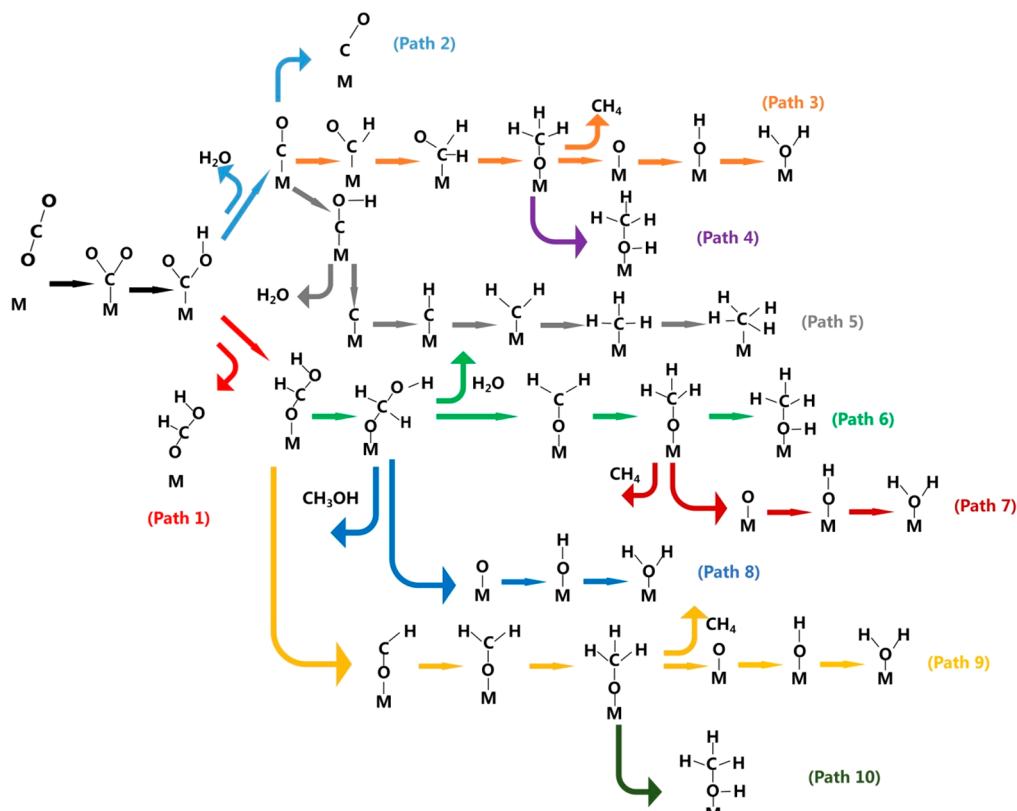


**Figure 3.** Schematic diagram of the CO<sub>2</sub>ERR pathways.

found that the optimal value of O atom on transition-metal diboride with highest catalytic activity for CO<sub>2</sub> electro-reduction is 0.64 eV.<sup>43</sup> Zou and Li's group found that the favorable adsorption energy of CO with the lowest reaction free energy of rate-determining step should locate in the region of 1.2–1.3 eV.<sup>44</sup> Table 1 shows the adsorption energies of CO<sub>2</sub> on metal-doped borophene, which varies from physisorption (0.20 eV on Pd/B) to chemisorption (1.53 eV on Os/B). The

different adsorption properties of reaction intermediates on the surface of catalysts will result in different reaction kinetics.

In this work, ten different CO<sub>2</sub>ERR reaction pathways were considered, which will form different final products, including carbon monoxide (CO), formic acid (HCOOH), water (H<sub>2</sub>O), methanol (CH<sub>3</sub>OH), and methane (CH<sub>4</sub>) (Figure 3). After the adsorption of CO<sub>2</sub>, a proton was first added to an O atom of CO<sub>2</sub> to form a carboxyl (COOH) intermediate. Then the carboxyl intermediate was hydrogenated to form CO

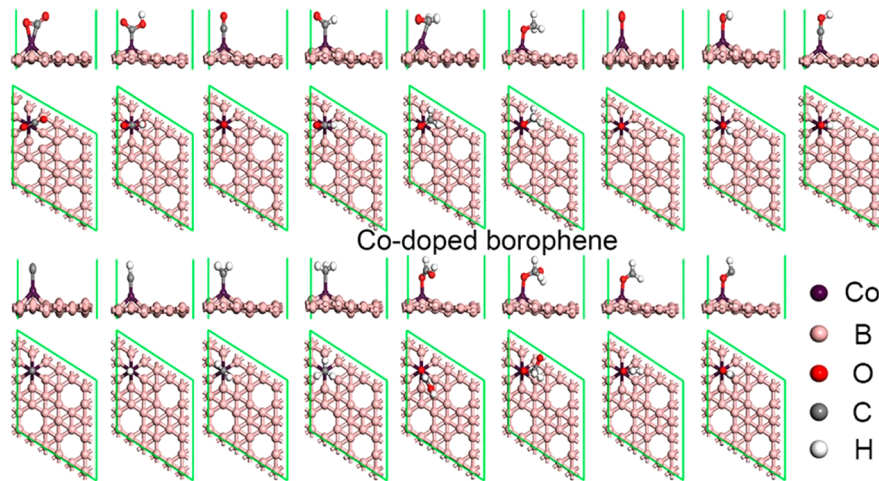


**Figure 4.** Optimized adsorption structures of CO<sub>2</sub>ERR intermediates on Co-doped borophene.

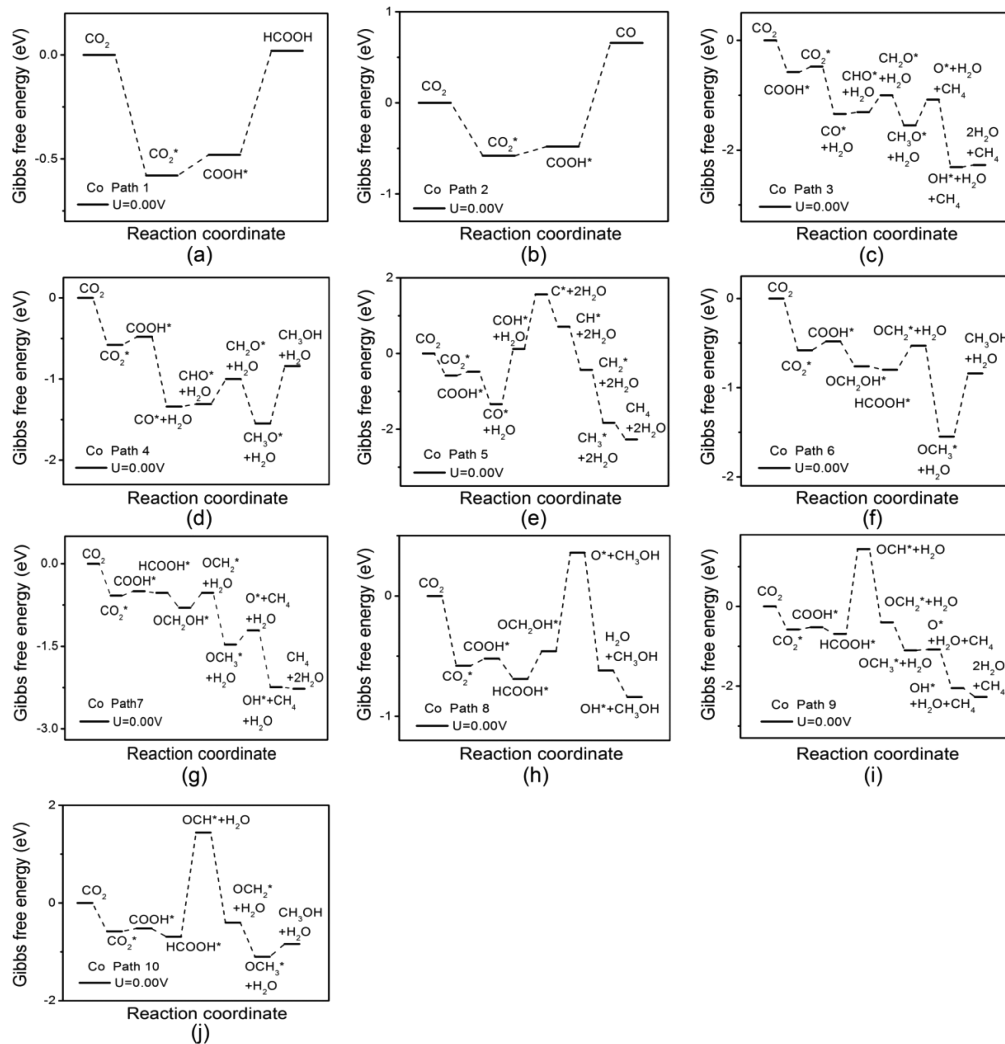


**Figure 5.** Free energy diagrams for CO<sub>2</sub>ERR on Co-doped borophene through ten different pathways.

and H<sub>2</sub>O (path 2), or was hydrogenated to form HCOOH (path 1). CO and HCOOH can desorb from the surface of catalyst as the final products or be further reduced.

Through the CO pathway, both C and O atoms can be hydrogenated to form a CHO intermediate or a COH

intermediate. The CHO intermediate can be further reduced to form CH<sub>4</sub> and H<sub>2</sub>O through eight coupled proton and electron transfer (CPET) steps (path 3) or be reduced to form CH<sub>3</sub>OH through six CPET steps (path 4). On the other side, the COH intermediate can be reduced to form H<sub>2</sub>O in the fifth

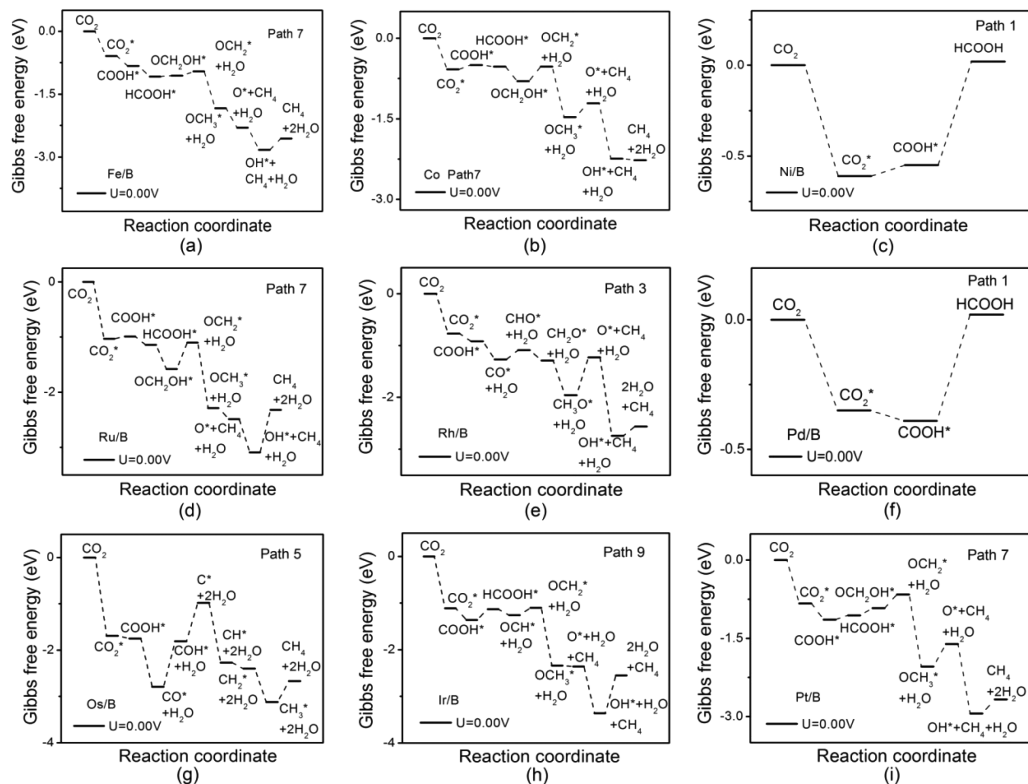


**Figure 6.** Free energy diagrams for  $\text{CO}_2\text{ERR}$  on metal-doped borophenes. The corresponding free energy diagrams are shown in Figures S6–S13 of Supporting Information.

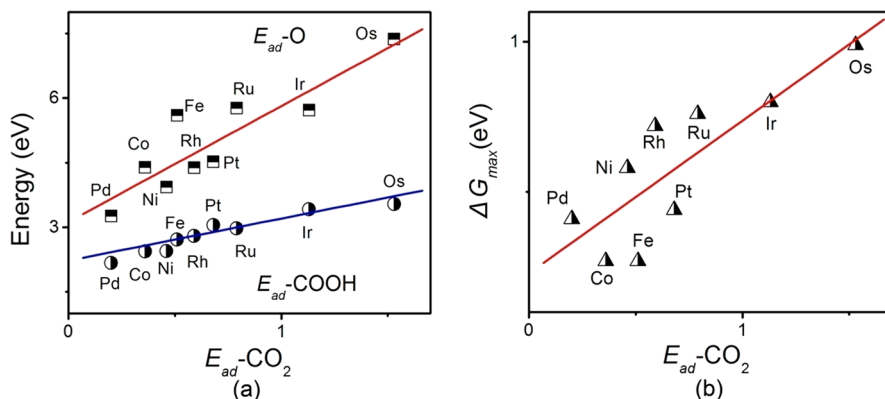


**Figure 7.** (a) Adsorption energies ( $E_{\text{ad}}$ ) of O and COOH plotted against the  $E_{\text{ad}}$  of  $\text{CO}_2$  on metal-doped borophene nanosheets. (b) The relationship between the  $\Delta G$  of the RDS in  $\text{CO}_2\text{ERR}$  and the  $E_{\text{ad}}$  of  $\text{CO}_2$  on metal-doped borophene nanosheets.

CPET step and then reduced to  $\text{CH}_4$  in the eighth CPET step (path 5).

Through the  $\text{HCOOH}$  pathway, the second proton can be added to the C atom to form an  $\text{OCH}_2\text{OH}$  intermediate or be added to the terminal O atom to form an OCH intermediate and a  $\text{H}_2\text{O}$  molecule. Once the  $\text{OCH}_2\text{OH}$  intermediate is formed, it can be reduced to  $\text{CH}_3\text{OH}$  (path 6),  $\text{CH}_4$  (path 7), or  $\text{CH}_3\text{OH}$  (path 8). By contrast, the OCH intermediate can be reduced to form  $\text{CH}_4$  (path 9) or  $\text{CH}_3\text{OH}$  (path 10).

The most stable adsorption structures of the  $\text{CO}_2\text{ERR}$  intermediates on metal-doped borophene nanosheets are shown in Figure 4 and Figures S3–S5 in Supporting Information, and their corresponding  $E_{\text{ad}}$  values are summarized in Table 1. It was found that  $\text{CO}_2\text{ERR}$  intermediates prefer to adsorb on the doped metal atoms, indicating that the doped metal atoms are the active sites during the  $\text{CO}_2\text{ERR}$ . To

better understand the energetically favorable mechanism, the Co-doped borophene nanosheet was taken as an example to show the favorable  $\text{CO}_2\text{ERR}$  mechanism. Figure 5 shows the free energy diagrams of the ten different mechanisms for Co-doped borophene nanosheet. It was found that the last step (the formation of  $\text{HCOOH}$ ) has a maximum  $\Delta G$  of 0.5 eV among all elementary steps in path 1. Therefore, the formation of  $\text{HCOOH}$  is the rate-determining step (RDS) in path 1. The formation of CO is the RDS of path 2 ( $\Delta G = 1.14$  eV), while the RDS of path 3 is the formation of  $\text{CH}_4$  ( $\Delta G = 0.47$  eV). The third step, the formation of COH, is the RDS in path 5 ( $\Delta G = 1.46$  eV), while the RDS in path 8 is the formation of the adsorbed O atom ( $\Delta G = 0.82$  eV). Paths 4 and 6 have the same RDS of the formation of  $\text{CH}_3\text{OH}$  ( $\Delta G = 0.71$  eV), and paths 9 and 10 have the same RDS of the formation of OCH ( $\Delta G = 2.13$  eV). The most important is that the RDS in path 7

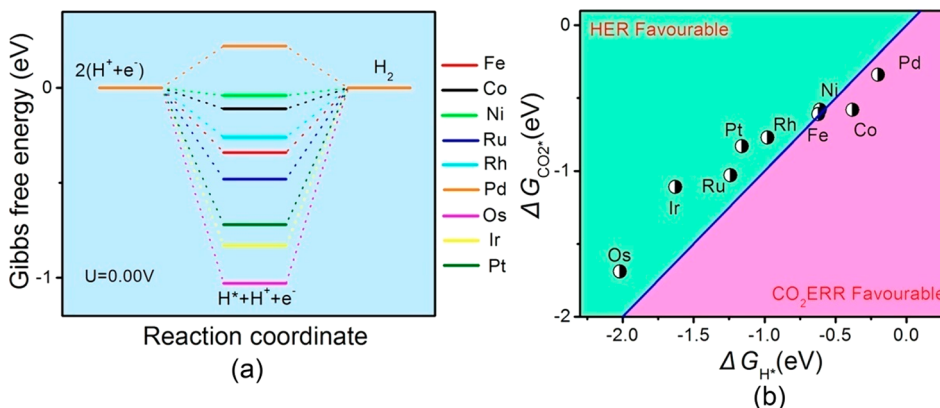


**Figure 8.** (a) Free energy diagrams for the HER on metal-doped borophenes. (b) Free energies for H and  $CO_2$  adsorption on metal-doped borophenes.

is the formation of the  $OCH_2$  intermediate with the  $\Delta G$  of 0.27 eV, which is much smaller than that of other pathways, indicating that path 7 is the preferred pathway on Co-doped borophene.

The optimal pathways for  $CO_2$ ERR on metal-doped borophene nanosheets are summarized in Figure 6. The favorable pathway of Rh-doped borophene nanosheet is path 3, and the corresponding RDS is the formation of  $CH_4$  with  $\Delta G$  values of 0.72 eV. Fe-, Co-, Ru-, and Pt-doped borophene nanosheets have the same favorable pathway of path 7, but their RDS is different. The RDS of Fe- and Ru-doped borophene is the formation of  $H_2O$  with  $\Delta G$  values of 0.27 and 0.76 eV, while the RDS of Co-doped borophene is the formation of  $OCH_2$  ( $\Delta G = 0.27$  eV). For Pt-doped borophene, the formation of  $CH_4$  is the RDS with  $\Delta G$  of 0.44 eV. Path 1 is the favored pathway of Ni- and Pd-doped borophene nanosheets, and the formation of  $HCOOH$  is the RDS with  $\Delta G$  values of 0.58 and 0.41 eV, respectively. For Os-doped borophene nanosheet, path 5 is the preferred pathway with the formation of  $COH$  as the RDS ( $\Delta G = 0.99$  eV). Moreover, the most favorable pathway of Ir-doped borophene was path 9, and the corresponding RDS is the formation of the second  $H_2O$  ( $\Delta G = 0.80$  eV). The  $\Delta G$  value of the RDS increases in the order of Co- = Fe- < Pd- < Pt- < Ni- < Rh- < Ru- < Ir- < Os-doped borophene, indicating that Fe-, Co-, and Pd-doped borophene nanosheets show the best  $CO_2$ ERR performance among the nine metal-doped borophene nanosheets. Our previous work found that Fe, Co, and Pd atoms prefer to adsorb on borophene separately rather than to form clusters, indicating that Fe, Co, and Pd atoms on borophene can avoid the aggregation.<sup>45</sup>

It can be concluded that the doped transition metals in borophene significantly influence the  $CO_2$ ERR catalytic performance and the favorable reaction pathway. It is interesting to note that the  $CO_2$ ERR on transition metal-doped borophene nanosheets exhibited a high selectivity to form  $CH_4$  or  $HCOOH$ , which results from the favorable reaction pathway on transition metal-doped borophene.  $CO_2$ ERR on Ni- and Pd-doped borophene nanosheets preferred to form  $HCOOH$  due to the favorable path 1, while  $CO_2$ ERR on other transition metal-doped borophenes exhibited a high selectivity to form  $CH_4$ . Note that the kinetic factors also play an important role for the product selectivity.<sup>46,47</sup> However, a facile approach to calculate the electrochemical barriers is lacking now. Therefore, in this work,

we try to understand the product selectivity from the viewpoint of thermodynamics.

It is well-known that the adsorption strength of reaction intermediates plays a critical role for the activity of the catalysts. In this work, a nearly linear relationship was observed among the adsorption energies of the reaction intermediates ( $CO_2$ , O, and  $COOH$ , Figure 7(a)). Therefore, the adsorption energy of  $CO_2$  can be used to characterize the catalytic activity of transition metal-doped borophene. As shown in Figure 7(b), a nearly linear relationship between the  $\Delta G$  value of the RDS and the adsorption energy of  $CO_2$  was found. However, the linear relationship is not very strict. This is due to the different transition metal-doped borophene nanosheets have different favorable pathways. Generally speaking, the  $\Delta G$  value of the RDS decreases as the decrease of the  $CO_2$  adsorption energy. The weak adsorption strength of reaction intermediates on metal-doped borophene nanosheets make it easier to form the final product and desorb from the surface of catalysts.

The hydrogen evolution reaction (HER) is a competitive reaction for  $CO_2$ ERR. To understand the selectivity between these two reactions, the reaction free energy of the first step involved in these two processes under the working potential of  $CO_2$ ERR (defined as the potential at which all elemental steps become exothermic) was used as a descriptor. If the free energy of the first step in the HER (H adsorption) under the working potential of  $CO_2$ ERR is lower than that for the first step involved in the  $CO_2$ ERR ( $CO_2$ adsorption), the active sites will be blocked by the adsorbed H atom, which will hamper the  $CO_2$ ERR process. The  $\Delta G$  value of the H adsorption under the working potential of  $CO_2$ ERR on Fe-, Co-, Ni-, Ru-, Rh-, Pd-, Os-, Ir-, and Pt-doped borophene nanosheets were calculated to be -0.61, -0.38, -0.62, -1.24, -0.98, -0.2, -2.02, -1.63, and -1.16 eV, respectively. As shown in Figure 8(b), it is clear that the adsorption of  $CO_2$  is more favorable than the adsorption of H in HER on Co- and Pd-doped borophene nanosheets, indicating that  $CO_2$ ERR on Co- and Pd-doped borophene nanosheets is more advantaged than HER.

#### 4. CONCLUSIONS

In this work, the catalytic performance of metal-doped borophenes ( $M = Fe, Co, Ni, Rh, Ru, Pd, Os, Ir, and Pt$ ) for  $CO_2$ ERR was studied based on DFT calculations. It was found that the  $CO_2$ ERR catalytic performance was closely related to the doped transition metal atoms, and different

transition metals resulted in different reaction kinetic properties and favorable reaction pathways. The  $\Delta G$  values of the RDS during the CO<sub>2</sub>ERR increase in the order: Co = Fe < Pd < Pt < Ni < Rh < Ru < Ir < Os. Co- and Pd-doped borophene nanosheets not only exhibit a high catalytic activity toward CO<sub>2</sub> reduction but also avoid the competitive HER. This work will help to understand the CO<sub>2</sub>ERR mechanism on transition-metal-doped borophene nanosheets and may provide guidance for the design of catalysts with high activity.

## ASSOCIATED CONTENT

### Supporting Information

The Supporting Information is available free of charge at <https://pubs.acs.org/doi/10.1021/acs.jpcc.0c05998>.

Additional experimental details as noted in the text ([PDF](#))

## AUTHOR INFORMATION

### Corresponding Author

**Xiuli Hou** — Institute for Advanced Materials, School of Materials Science and Engineering, Jiangsu University, Zhenjiang 212013, China;  [orcid.org/0000-0003-4963-682X](http://orcid.org/0000-0003-4963-682X); Email: [xiulihou@foxmail.com](mailto:xiulihou@foxmail.com)

### Authors

**Xuejian Xu** — Institute for Advanced Materials, School of Materials Science and Engineering, Jiangsu University, Zhenjiang 212013, China

**Jiajie Lu** — Institute for Advanced Materials, School of Materials Science and Engineering, Jiangsu University, Zhenjiang 212013, China

**Peng Zhang** — Institute for Advanced Materials, School of Materials Science and Engineering, Jiangsu University, Zhenjiang 212013, China

**Beibei Xiao** — School of Energy and Power Engineering, Jiangsu University of Science and Technology, Zhenjiang 212003, China;  [orcid.org/0000-0001-9637-7512](http://orcid.org/0000-0001-9637-7512)

**Jianli Mi** — Institute for Advanced Materials, School of Materials Science and Engineering, Jiangsu University, Zhenjiang 212013, China;  [orcid.org/0000-0001-6454-5040](http://orcid.org/0000-0001-6454-5040)

Complete contact information is available at:

<https://pubs.acs.org/10.1021/acs.jpcc.0c05998>

### Notes

The authors declare no competing financial interest.

## ACKNOWLEDGMENTS

This work was supported by the financial support from the National Natural Science Foundation of China (grant no. 21403092), the Special Financial Grant from the China Postdoctoral Science Foundation (2015T80506), Natural Science Fund for Colleges and Universities in Jiangsu Province (17KJB430008), International Postdoctoral Exchange Fellowship Program 2016, and the Senior Intellectuals Fund of Jiangsu University (nos. 12JDG094 and 13JDG032).

## REFERENCES

- (1) Scott, V.; Gilfillan, S. M.; Markusson, N.; Chalmers, H.; Haszeldine, R. S. Last Chance for Carbon Capture and Storage. *Nat. Clim. Change* **2013**, *3*, 105–111.
- (2) Lashof, D. A.; Ahuja, D. R. Relative Contributions of Greenhouse Gas Emissions to Global Warming. *Nature* **1990**, *344*, 529–531.
- (3) Bu, Y. F.; Zhao, M.; Zhang, G. X.; Zhang, X.; Gao, W.; Jiang, Q. Electroreduction of CO<sub>2</sub> on Cu Clusters: The Effects of Size, Symmetry, and Temperature. *ChemElectroChem* **2019**, *6*, 1831–1837.
- (4) Haszeldine, R. S. Carbon Capture and Storage: How Green Can Black Be? *Science* **2009**, *325*, 1647–1652.
- (5) Qi, L.; Liu, S.; Gao, W.; Jiang, Q. Mechanistic Understanding for CO<sub>2</sub> Electroreduction on Cu<sub>2</sub>O. *J. Phys. Chem. C* **2018**, *122*, 5472–5480.
- (6) Koper, M. T. M. Thermodynamic Theory of Multi-electron Transfer Reactions: Implications for Electrocatalysis. *J. Electroanal. Chem.* **2011**, *660*, 254–260.
- (7) Nie, X.; Luo, W.; Janik, M. J.; Asthagiri, A. Reaction Mechanisms of CO<sub>2</sub> Electrochemical Reduction on Cu(111) Determined with Density Functional Theory. *J. Catal.* **2014**, *312*, 108–122.
- (8) Liu, S. P.; Zhao, M.; Gao, W.; Jiang, Q. Mechanistic Insights into the Unique Role of Copper in CO<sub>2</sub> Electroreduction Reactions. *ChemSusChem* **2017**, *10*, 387–393.
- (9) Lim, R. J.; Xie, M.; Sk, M. A.; Lee, J. M.; Fisher, A.; Wang, X.; Lim, K. H. A Review on the Electrochemical Reduction of CO<sub>2</sub> in Fuel Cells, Metal Electrodes and Molecular Catalysts. *Catal. Today* **2014**, *233*, 169–180.
- (10) Trickett, C. A.; Helal, A.; Al-Maythalony, B. A.; Yamani, Z. H.; Cordova, K. E.; Yaghi, O. M. The Chemistry of Metal–organic Frameworks for CO<sub>2</sub> Capture, Regeneration and Conversion. *Nat. Rev. Mater.* **2017**, *2*, 17045.
- (11) Dang, W. J.; Shen, Y. Q.; Lin, M.; Jiao, H.; Xu, L.; Wang, Z. L. Noble-metal-free Electrocatalyst Based on a Mixed CoNi Metal-organic Framework for Oxygen Evolution Reaction. *J. Alloys Compd.* **2019**, *792*, 69–76.
- (12) Li, H.; Wang, M.; Luo, L.; Zeng, J. Static Regulation and Dynamic Evolution of Single-Atom Catalysts in Thermal Catalytic Reactions. *Adv. Sci.* **2019**, *6*, 1801471.
- (13) Wan, G.; Yu, P.; Chen, H.; Wen, J.; Sun, C.; Zhou, H.; Zhang, N.; Li, Q.; Zhao, W.; Xie, B.; et al. Engineering Single-Atom Cobalt Catalysts toward Improved Electrocatalysis. *Small* **2018**, *14*, 1704319.
- (14) Zhang, H.; Liu, G.; Shi, L.; Ye, J. Single-Atom Catalysts: Emerging Multifunctional Materials in Heterogeneous Catalysis. *Adv. Energy. Mater.* **2018**, *8*, 1701343.
- (15) Esrafilo, M. D.; Nejaddehrahimi, B. Theoretical Insights into Hydrogenation of CO<sub>2</sub> to Formic Acid Over a Single Co Atom Incorporated Nitrogen-doped Graphene: a DFT Study. *Appl. Surf. Sci.* **2019**, *475*, 363–371.
- (16) Zhao, C.; Zhang, G.; Gao, W.; Jiang, Q. Single Metal Atoms Regulated Flexibly by a 2D InSe Substrate for CO<sub>2</sub> Reduction Electrocatalysts. *J. Mater. Chem. A* **2019**, *7*, 8210–8217.
- (17) Jeong, H. Y.; Balamurugan, M.; Choutipalli, V. S. K.; Jo, J.; Baik, H.; Subramanian, V.; Kim, M.; Sim, U.; Nam, K. T. Tris(2-benzimidazolylmethyl)amine-directed Synthesis of Single-atom Nickel Catalysts for Electrochemical CO Production From CO<sub>2</sub>. *Chem. - Eur. J.* **2018**, *24*, 18444–18454.
- (18) Wang, Z.; Zhao, J.; Cai, Q. CO<sub>2</sub> Electroreduction Performance of a Single Transition Metal Atom Supported on Porphyrin-like Graphene: a Computational Study. *Phys. Chem. Chem. Phys.* **2017**, *19*, 23113–23121.
- (19) Liu, J.-H.; Yang, L.-M.; Ganz, E. Electrochemical Reduction of CO<sub>2</sub> by Single Atom Catalysts TM-TCNQ Monolayers. *J. Mater. Chem. A* **2019**, *7*, 3805–3814.
- (20) Novoselov, K. S.; Geim, A. K.; Morozov, S. V.; Jiang, D.; Katsnelson, M. I.; Grigorieva, I. V.; Dubonos, S. V.; Firsov, A. A. Two-Dimensional Gas of Massless Dirac Fermions in Graphene. *Nature* **2005**, *438*, 197–200.
- (21) Jiang, Q.; Zhang, J.; Ao, Z.; Huang, H.; He, H.; Wu, Y. First Principles Study on the CO Oxidation on Mn-Embedded Divacancy Graphene. *Front. Chem.* **2018**, *6*, 187.
- (22) Li, H.; Wu, Y.; Li, L.; Gong, Y.; Niu, L.; Liu, X.; Wang, Y.; Sun, C.; Li, C. Adjustable Photocatalytic Ability of Monolayer g-C3N4

- Utilizing Single-metals Atom: Density Functional Theory. *Appl. Surf. Sci.* **2018**, *457*, 735–744.
- (23) Chen, X.; Liu, J.; Zhang, W.; Xiao, B.; Zhang, P.; Li, L. First-Principles Study on the Mechanism of Hydrogen Decomposition and Spillover on Borophene. *J. Phys. Chem. C* **2017**, *121*, 17314–17320.
- (24) Piazza, Z. A.; Hu, H.-S.; Li, W.-L.; Zhao, Y.-F.; Li, J.; Wang, L.-S. Planar Hexagonal  $B_{36}$  as a Potential Basis for Extended Single-atom Layer Boron Sheets. *Nat. Commun.* **2014**, *5*, 3113.
- (25) Penev, E. S.; Bhowmick, S.; Sadzadeh, A.; Yakobson, B. I. Polymorphism of Two-Dimensional Boron. *Nano Lett.* **2012**, *12*, 2441–2445.
- (26) Mannix, A. J.; Zhou, X.; Kiraly, B.; Wood, J. D.; Alducin, D.; Myers, B. D.; Liu, X.; Fisher, B. L.; Santiago, U.; Guisinger, N. P.; et al. Synthesis of Borophenes: Anisotropic, Two-dimensional Boron Polymorphs. *Science* **2015**, *350*, 1513–1516.
- (27) Wang, Z.; Lu, T.; Wang, H.; Feng, Y. P.; Zheng, J. Review of Borophene and its Potential Applications. *Front. Phys. China* **2019**, *14*, 33403.
- (28) Shen, H.; Li, Y.; Sun, Q. Cu Atomic Chains Supported on  $\beta$ -borophene Sheets for Effective  $CO_2$  Electroreduction. *Nanoscale* **2018**, *10*, 11064–11071.
- (29) Liu, C.; Li, Q.; Zhang, J.; Jin, Y.; Macfarlane, D. R.; Sun, C. Theoretical Evaluation of Possible 2D Boron Monolayer in  $N_2$  Electrochemical Conversion into Ammonia. *J. Phys. Chem. C* **2018**, *122*, 25268–25273.
- (30) Wang, L.; Chen, X.; Du, H.; Yuan, Y.; Qu, H.; Zou, M. First-principles Investigation on Hydrogen Storage Performance of Li, Na and K Decorated Borophene. *Appl. Surf. Sci.* **2018**, *427*, 1030–1037.
- (31) Delley, B. An All-electron Numerical Method for Solving the Local Density Functional for Polyatomic Molecules. *J. Chem. Phys.* **1990**, *92*, 508–517.
- (32) Perdew, J. P.; Burke, K.; Ernzerhof, M. Generalized Gradient Approximation Made Simple. *Phys. Rev. Lett.* **1996**, *77*, 3865–3868.
- (33) Koelling, D. D.; Harmon, B. N. A Technique for Relativistic Spin-polarised Calculations. *J. Phys. C: Solid State Phys.* **1977**, *10*, 3107–3114.
- (34) Grimme, S. Semiempirical GGA-type Density Functional Constructed with a Long-range Dispersion Correction. *J. Comput. Chem.* **2006**, *27*, 1787–1799.
- (35) Yao, M.; Ji, Y.; Wang, H.; Ao, Z.; Li, G.; An, T. Adsorption Mechanisms of Typical Carbonyl-containing Volatile Organic Compounds on Anatase  $TiO_2$  (001) Surface: A DFT Investigation. *J. Phys. Chem. C* **2017**, *121*, 13717–13722.
- (36) Liu, W.; Tkatchenko, A.; Scheffler, M. Modeling Adsorption and Reactions of Organic Molecules at Metal Surfaces. *Acc. Chem. Res.* **2014**, *47*, 3369–3377.
- (37) Rossmeisl, J.; Nørskov, J. K.; Taylor, C. D.; Janik, M. J.; Neurock, M. Calculated Phase Diagrams for the Electrochemical Oxidation and Reduction of Water Over Pt(111). *J. Phys. Chem. B* **2006**, *110*, 21833–21839.
- (38) Wu, Y.; Li, C.; Liu, W.; Li, H.; Gong, Y.; Niu, L.; Liu, X.; Sun, C.; Xu, S. Unexpected Monoatomic Catalytic-host Synergetic OER/ORR by Graphitic Carbon Nitride: Density Functional Theory. *Nanoscale* **2019**, *11*, 5064–5071.
- (39) Tak, Y. J.; Yang, S.; Lee, H.; Lim, D.; Soon, A. Examining the Rudimentary Steps of the Oxygen Reduction Reaction on Single-atomic Pt Using Ti-based Non-oxide Supports. *J. Ind. Eng. Chem.* **2018**, *58*, 208–215.
- (40) Nørskov, J. K.; Rossmeisl, J.; Logadottir, A. A.; Lindqvist, L.; Kitchin, J. R.; Bligaard, T.; Jonsson, H. Origin of the Overpotential for Oxygen Reduction at a Fuel-Cell Cathode. *J. Phys. Chem. B* **2004**, *108*, 17886–17892.
- (41) Delley, B. The Conductor-like Screening Model for Polymers and Surfaces. *Mol. Simul.* **2006**, *32*, 117–123.
- (42) Trinh, Q. T.; Yang, J.; Lee, J. Y.; Saey, M. Computational and Experimental Study of the Volcano Behavior of the Oxygen Reduction Activity of  $PdM@PdPt/C$  ( $M = Pt, Ni, Co, Fe$ , and Cr) Core-shell Electrocatalysts. *J. Catal.* **2012**, *291*, 26–35.
- (43) Yuan, H.; Li, Z.; Yang, J. Transition-Metal Diboride: A New Family of Two-Dimensional Materials Designed for Selective  $CO_2$  Electroreduction. *J. Phys. Chem. C* **2019**, *123*, 16294–16299.
- (44) Zhou, H.; Zou, X.; Wu, X.; Yang, X.; Li, J. Coordination Engineering in Cobalt-Nitrogen-Functionalized Materials for  $CO_2$  Reduction. *J. Phys. Chem. Lett.* **2019**, *10*, 6551–6557.
- (45) Zhang, P.; Xu, X.; Song, E.; Hou, X.; Yang, X.; Mi, J.; Huang, J.; Stampfl, C. Transition Metal-Doped  $\alpha$ -Borophene as Potential Oxygen and Hydrogen Evolution Electrocatalyst: A Density Functional Theory Study. *Catal. Commun.* **2020**, *144*, 106090.
- (46) Yoo, J. S.; Christensen, R.; Vegge, T.; Nørskov, J. K.; Studt, F. Theoretical Insight into the Trends that Guide the Electrochemical Reduction of Carbon Dioxide to Formic Acid. *ChemSusChem* **2016**, *9*, 358–363.
- (47) Feaster, J. T.; Shi, C.; Cave, E. R.; Hatsukade, T.; Abram, D. N.; Kuhl, K. P.; Hahn, C.; Nørskov, J. K.; Jarillo, T. F. Understanding Selectivity for the Electrochemical Reduction of Carbon Dioxide to Formic Acid and Carbon Monoxide on Metal Electrodes. *ACS Catal.* **2017**, *7*, 4822–4827.